METROLOGY AND MEASUREMENT SYSTEMS
Index 330930, ISSN 0860-8229
www.metrology.pg.gda.pl

SYNCHRONOUS MEASUREMENT OF OUT-OF-PLANE DISPLACEMENT AND SLOPES BY TRIPLE-OPTICAL-PATH DIGITAL SPECKLE PATTERN INTERFEROMETRY

Guo-Qing Gu, Gui-Zhong Xu, Bing Xu

Yancheng Institute of Technology, School of Civil Engineering, Yancheng, 224051, China
(✉ *gqgu@ycit.edu.cn*, +86 138 1557 9084)

Abstract

This study proposes a triple-optical-path digital speckle pattern interferometry (DSPI) setup for measuring the full-field out-of-plane displacement and two orthogonal slopes simultaneously as well as independently. The designed setup contains one conventional out-of-plane speckle interferometer and two orthogonal modified shearographic interferometers with dual-observation geometry. In the setup, one laser device is used as the coherent source, and three monochrome cameras placed along a single line are used as the image acquisition device. Three correlation fringe patterns, one out-of-plane displacement fringe pattern and two slope fringe patterns, are captured synchronously by three cameras, and then are analysed using the phase-shifting technique to extract the phase distributions. The examinations of a practical non-contact measurement and a non-destructive testing (NDT) application by using the proposed setup are carried out in this study.

Keywords: simultaneous displacement and slopes measurement, non-destructive testing, digital speckle pattern interferometry, shearography, triple-optical-path.

1. Introduction

Both the out-of-plane displacement and its orthogonal slope components, which can be translated further into curvature and twist distributions, are the crucial parameters for the loaded structures' strength prediction and performance estimation [1]. Consequently, simultaneous, direct as well as accurate measurement of the out-of-plane displacement and its orthogonal slopes is of vital importance, and is also urgently required in many fields, especially in automobile and aerospace industries.

Optical measurement methods, such as digital holography (DH), digital image correlation (DIC), profilometry, digital speckle pattern interferometry (DSPI), digital shearography (DS), and so on, have become widely accepted tools for measuring surface deformation, slope, strain, profile, and so on. Due to rapid development of both electronic devices and digital image processing techniques, optical measurement methods have now reached a great progress. For example, DH has been proven to be quite suitable for deformation and strain measurements owing to its characteristics of high precision and high contrast [2, 3]. However, DH is so sensitive to environmental changes that it cannot be used outdoors. Nowadays, DIC is a popular, powerful and

Article history: received on Jun. 13, 2017; accepted on Oct. 05, 2017; available online on Mar. 26, 2018, DOI: 10.24425/118159.

robust optical tool for quantitative measurement of deformations and strains [4, 5]. However, it is quite difficult to attain a balance between measurement accuracy and computational speed. As for optical profilometry or topography, it has mainly been employed for quantitative inspection of surface profile or surface roughness [6–8], while it has rarely been used for measurement of surface deformations and slopes. Both DSPI and DS are widely accepted optical measurement techniques due to the advantages of high-precision, non-contact, and full-field measurement [9–11]. The former is mainly focused on the measurement of surface in-plane or out-of-plane displacements, whereas the latter is usually used for measuring surface strains or slopes, which can be well suited for non-destructive testing (NDT). With the help of various temporal and spatial phase-shifting techniques, both deformations and slopes can be accurately measured by these two techniques [12]. If the simultaneous measurement of displacement and its orthogonal slopes is required, only DSPI or DS can not reach the goal due to the fact that numerical differentiation or integration of the measured quantities is prone to errors. In such cases, a combination of DSPI and DS is preferred.

Previously, many DSPI configurations have been proposed for the measurement of out-of-plane displacement and its slope for a single system [13–15]. However, these methods need to switch over from the out-of-plane measurement to the slope measurement or vice versa – to achieve the measurement of out-of-plane displacement and its slope. In essence, they just measure these two independent quantities successively, rather than simultaneously. In order to attain the simultaneous measurement of out-of-plane displacement and its slope, Mohan et al. firstly proposed a DSPI configuration requiring a specific reference wave, which combined the out-of-plane displacement configuration and the shearography configuration [16]. In spite of being able to simultaneously measure the out-of-plane displacement and slope, this configuration cannot fully use the whole resolution of detector. Later, optical setups based on DSPI or DS with the spatial phase-shifting technique were presented for the simultaneous measurement of out-of-plane displacement and its slope [17–19]. Among them, the application of spatial carrier frequency technique makes it possible to achieve the ability of dynamic measurement. Although these optical configurations successfully accomplish the simultaneous measurement of out-of-plane displacement and slope using only one detector, a relatively lower spatial resolution offered by the spatial carrier frequencies technique leads to unsatisfactory measurement accuracy. Moreover, these methods can perform the simultaneous measurement of out-of-plane displacement and its slope only in one direction.

Recently, several optical setups based on DS have been proposed for simultaneous measurement of slopes in two orthogonal directions. For example, a DS setup based on the modified Michelson interferometer using three beam splitters and two switches has been applied to obtaining two orthogonal slopes sequentially [20]. Lately, DS configurations with multiple wavelengths and a colour camera have been used for the simultaneous measurement of two orthogonal strains or slopes [21, 22]. However, the limits of these setups are quite obvious. On the one hand, these setups do not take the out-of-plane displacement measurement into consideration. On the other hand, the designed measurement setups usually become either complex or expensive due to the use of multi-wavelength and colour detector. Overall, in order to measure the out-of-plane displacement and its two orthogonal slopes simultaneously, there are often employed two measurement strategies. One method is to adopt DSPI to measure the out-of-plane displacement firstly. Then, the slopes in two orthogonal directions are, respectively, measured directly through differentiation. In this case, the differentiation process inevitably expands the measurement error induced by random speckle noise to decrease the slopes' measurement accuracy. Another method combines two shearographic interferometers and an out-of-plane speckle interferometer to form an integrated triple-optical-path DSPI system for measurement of multiple quantities. Although

this method certainly makes the optical system become relatively complex, the merit is that both out-of-plane displacement and its two orthogonal slopes can be indeed determined simultaneously and independently. Therefore, there is a great need to simplify the integrated system to perform the simultaneous measurement of out-of-plane displacement and its two orthogonal slopes.

A construction of novel synchronous triple-optical-path DSPI system has been presented in this paper, which greatly simplifies the whole optical system. Differently from the existing DSPI or DS systems for the simultaneous measurement of out-of-plane displacement and slope, three monochrome charged couple device (CCD) cameras and only one wavelength have been adopted in this system to perform the simultaneous measurement of desired three independent quantities corresponding to one out-of-plane displacement and two orthogonal slopes, respectively.

2. Measurement principle

The optical arrangement for simultaneous determining out-of-plane displacement and its orthogonal slopes of a bent thin plate by using the synchronous triple-optical-path DSPI system is shown in Fig. 1. In the system, three different optical paths corresponding to two shearographic interferometers and one out-of-plane interferometer, can be obtained separately. Thus, three independent quantities can be measured simultaneously. An expanded laser beam perpendicularly illuminates the beam splitter (BS), and then is divided into two beams. In the horizontal plane (i.e. *xoz* plane), one reflective beam directly illuminates the tested object surface, and the other transmission beam illuminates the diffusing reference plane (RP). Both reflective wave-front scattered from RP and object wave-front scattered from the tested object surface are combined coherently in the image plane of the first CCD (CCD1) to generate a speckle-gram representing the out-of-plane displacement (w). Meanwhile, the pair of plane reflective mirrors (M1 and M2) and the front surface of coated right angle prism (P1) assembly provides two symmetrical optical paths, which means that the same point of the object will be imaged along two different paths. If one of the mirrors is artificially tilted, a lateral shear along *x*direction can be easily introduced so that the second CCD (CCD2) can record two slightly sheared images. In this way, the scattered wave-fronts from two adjacent points of the object are collected by two paths to interfere

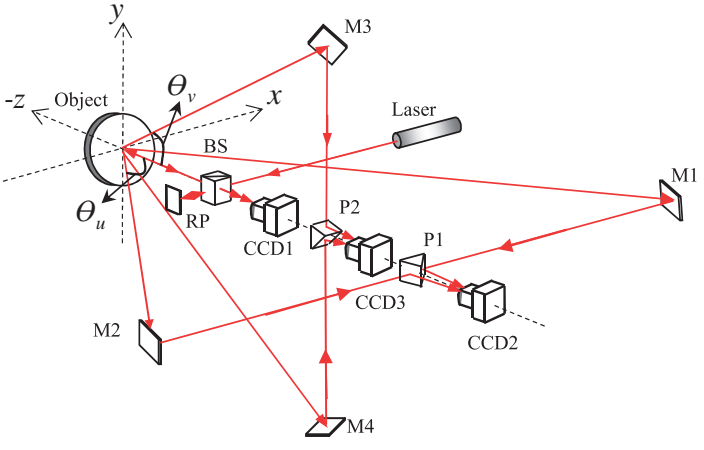

Fig. 1. A schematic of the synchronous triple-optical-path DSPI system (CCD: charged couple device; RP: reference plane; BS: beam splitter; P: prism; M: mirror).

in the image plane on CCD2 to produce a shearogram corresponding to the slope in x direction $(\partial w/\partial x)$. Likewise, in the vertical plane (i.e. yoz plane), a shearogram corresponding to the slope in $y$direction $(\partial w/\partial y)$ can also be generated in the image plane on the third CCD (CCD3) by introducing the shear along y direction.

2.1. Measurement of out-of-plane displacement

According to the difference between the observation and illumination unit vectors $\mathbf{K}_o$ and $\mathbf{K}_e$, respectively, a relative phase change δ due to object deformation can be expressed as [12]

$$\delta = \frac{2\pi}{\lambda}(\mathbf{K}_o - \mathbf{K}_e)\cdot\mathbf{d} = \frac{2\pi}{\lambda}\mathbf{s}\cdot\mathbf{d}, \tag{1}$$

where λ is a wavelength of the employed laser, $\mathbf{s}$ is a sensitivity vector reflecting the relationship between the directions of observation and illumination, and $\mathbf{d}$ is a displacement vector at any point of the object: $\mathbf{d} = u\mathbf{i} + v\mathbf{j} + w\mathbf{k}$, u, v, w are displacement components along x, y, z directions, respectively, as shown in Fig. 1. In respect to the out-of-plane displacement measurement, a phase difference δ_w can be further rewritten as

$$\delta_w = \frac{4\pi}{\lambda}w. \tag{2}$$

It can be easily obtained from Eq. (2) that one fringe corresponds to a displacement of $\lambda/2$, and the setup's measurement sensitivity to out-of-plane displacement depends only on the wavelength of laser source used in the proposed setup, and has nothing to do with other parameters.

2.2. Measurement of slope

According to Eq. (1), a phase difference δ_x between the sheared scattered wave-fronts in xoz plane due to object deformation can be expressed as

$$\begin{aligned}\delta_x &= \frac{2\pi}{\lambda}\left[(\mathbf{K}_{o1} - \mathbf{K}_e)\cdot\mathbf{d}(x+\Delta_x, y) - (\mathbf{K}_{o2} - \mathbf{K}_e)\cdot\mathbf{d}(x,y)\right] \\ &= \frac{2\pi}{\lambda}\left[(\mathbf{K}_{o1} - \mathbf{K}_e)\cdot\mathbf{d}(x+\Delta_x, y) - (\mathbf{K}_{o1} - \mathbf{K}_e)\cdot\mathbf{d}(x,y)\right. \\ &\quad \left. + (\mathbf{K}_{o1} - \mathbf{K}_e)\cdot\mathbf{d}(x,y) - (\mathbf{K}_{o2} - \mathbf{K}_e)\cdot\mathbf{d}(x,y)\right] \\ &= \frac{2\pi}{\lambda}\left[(\mathbf{K}_{o1} - \mathbf{K}_e)\cdot\frac{\partial\mathbf{d}(x,y)}{\partial x}\Delta_x + (\mathbf{K}_{o1} - \mathbf{K}_{o2})\cdot\mathbf{d}(x,y)\right],\end{aligned} \tag{3}$$

where $\mathbf{d}(x+\Delta_x, y)$, $\mathbf{d}(x,y)$ are displacement vectors in points $(x+\Delta_x, y)$ and (x,y), respectively, and Δ_x is a shearing distance along x direction. As indicated in Fig. 1, $\mathbf{K}_e$, $\mathbf{K}_{o1}$, $\mathbf{K}_{o2}$ can be written as

$$\begin{aligned}\mathbf{K}_e &= -\mathbf{k}, \\ \mathbf{K}_{o1} &= \sin\theta_u\mathbf{i} + \cos\theta_u\mathbf{k}, \\ \mathbf{K}_{o2} &= -\sin\theta_u\mathbf{i} + \cos\theta_u\mathbf{k}.\end{aligned} \tag{4}$$

Therefore, based on Eq. (4), Eq. (3) can be rewritten as

$$\delta_x = \frac{2\pi}{\lambda}\left\{2u\sin\theta_u + \left[\sin\theta_u\frac{\partial u}{\partial x} + (1+\cos\theta_u)\frac{\partial w}{\partial x}\right]\Delta_x\right\}, \tag{5}$$

where $\partial w/\partial x$, $\partial u/\partial x$ are the first order partial derivatives of out-of-plane displacement and in-plane displacement of the deformed object, and θ_u is an inclined angle in respect to the surface normal in *xoz* plane. In Eq. (5), three terms are responsible for fringe formation. The third term contains the slope $(\partial w/\partial x)$ information, while the first and second terms are the in-plane displacement (u) and in-plane strain $(\partial u/\partial x)$ components, respectively. If the in-plane displacement can be neglected $(u = 0)$, the former two terms will have no effect on the slope $(\partial w/\partial x)$ information. According to this condition, Eq. (5) can be further rewritten as

$$\delta_x = \frac{2\pi}{\lambda}\left[(1+\cos\theta_u)\frac{\partial w}{\partial x}\right]\Delta_x\,. \tag{6}$$

Eq. (6) shows that one slope fringe corresponds to a derivative of $\lambda/[(1+\cos\theta_u)\Delta x]$. The proposed setup has an advantage of flexibility in choosing both θ_u and Δ_x which, apart from λ, are the other two sensitivity-determining parameters of the setup. With an increase of either of them, the setup's measurement sensitivity to slope may be enhanced accordingly. Similarly, the slope in *y* direction $(\partial w/\partial y)$ can also be obtained by introducing the shear along *y* direction.

As indicated by Eqs. (2), (6), the phase information must be extracted for measuring w and $\partial w/\partial x$ (or $\partial w/\partial y$). To obtain the phase information from the speckle fringe patterns, a phase-shifting technique must be introduced in the proposed optical system. Here, the four-step phase-shifting technique with a phase step value of $\pi/2$ is employed for phase extraction. Due to the fact that the resulting wrapped phase distributions are excessively noisy, the noise can be substantially reduced by using a Fast Discrete Curve-let Transform (FDCT)-based filtering procedure [23]. In addition, a process of phase unwrapping is also required to remove 2π-phase discontinuities by the addition or subtraction of multiples of 2π to/from each phase value. Here, the quality-guided unwrapping algorithm is used for phase unwrapping to obtain smooth and continuous phase distributions [24].

3. Experimental results and discussion

3.1. Experimental setup and procedures

Fig. 2 shows a photo of the practical experimental setup illustrated in Fig. 1. All pieces of experimental equipment were fixed on a vibration-proof precise optical table to avoid environmental disturbance. A He-Ne laser, with a wavelength of 632.8 nm and a maximum power of 50 mW, was employed as a coherent light source to illuminate the tested specimen surface normally. Three monochrome CCD cameras (Point Grey Flea2) were placed along a single line to capture speckle fringe patterns synchronously. The temporal phase-shifting technique was implemented using the classical four-step algorithm for extracting multiple phase information that was introduced by employing piezoelectric transducer (PZT) devices mounted on the rear of both the reference plane and mirrors to control the phase-shifting and to interface to a computer with an IEEE-1394b video grabber card with three video capture ports.

To verify the feasibility and effectiveness of the proposed synchronous triple-optical-path DSPI system shown in Fig. 2, an experimental measurement of a circular thin aluminium alloy plate with a radius of 50 mm and a thickness of 4 mm was performed. The specimen with its edge clamped was loaded centrally by a screw micro-meter, so that an out-of-plane deformation was made at the specimen surface. Prior to accomplishing the experiment, the specimen surface was coated with white paint to increase the scattered light intensity and contrast

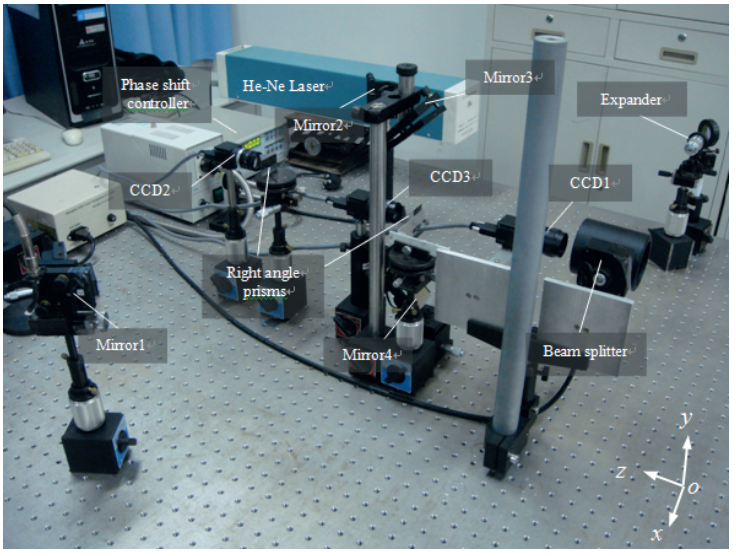

Fig. 2. A photo of the experimental setup illustrated in Fig. 1.

of the speckle fringe patterns. The specimen was placed perpendicularly to three CCD cameras and the light from the beam splitter. The focuses of three CCD cameras were adjusted to acquire three clear images of the specimen surface. The optical paths were adjusted and the distances of each pair of reflection mirrors in orthogonal directions were regulated. θ_u and θ_v shown in Fig. 1 were approximately 16° and 6° according to the geometric measurement. Then, one of the mirrors in *xoz* (or *yoz*) plane was deliberately tilted to produce two slightly displaced images viewed on CCD2 (or CCD3), and the shearing distances in orthogonal directions were adjusted to be about 12 mm – in this case based on the geometric calculations. The specimen surface was then subjected to an out-of-plane displacement of 2.2 μm at the centre, due to the fact that the screw micrometer pushed the centre of the specimen surface from the back side. Finally, a series of speckle-grams were synchronously recorded by three CCD cameras.

3.2. Measurement results and analysis

During the testing, the real-time visible speckle fringe patterns corresponding to the contours of w-field, $\partial w/\partial x$-field and $\partial w/\partial y$-field are generated both simultaneously and independently, and are, respectively, shown in Fig. 3a, b, and c. It can be found that the fringe patterns have a high contrast. For slope measurements, it is assumed that the in-plane displacement under this loading is approximately equal to zero. As a result, Fig. 3b and c represent the pure slope changes of the specimen surface in two orthogonal directions, respectively. Afterwards, the four-step phase-shifting method with a phase step value of $\pi/2$ is applied to extracting phase maps, and the wrapped phase maps for the out-of-plane displacement and its slopes, after filtering by FDCT, are shown in Fig 4a, b, and c, respectively. Obviously, the random speckle noise in the wrapped phase maps is significantly reduced. Furthermore, by means of the quality-guided unwrapping algorithm, the continuous three-dimensional distributions associated with the displacement and slopes obtained from Eq. (2) and Eq. (6) are shown in Fig. 5a, b, and c, respectively.

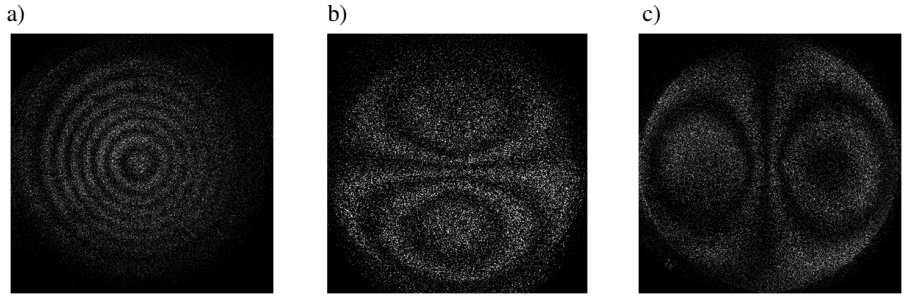

Fig. 3. Real-time speckle fringe patterns due to a central loading: a) w-field; b) $\partial w/\partial x$-field; c) $\partial w/\partial y$-field.

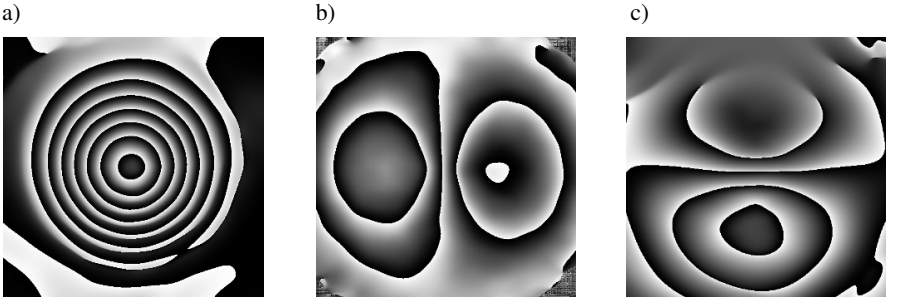

Fig. 4. FDCT-based filtered wrapped phase maps: a) w-field; b) $\partial w/\partial x$-field; c) $\partial w/\partial y$-field.

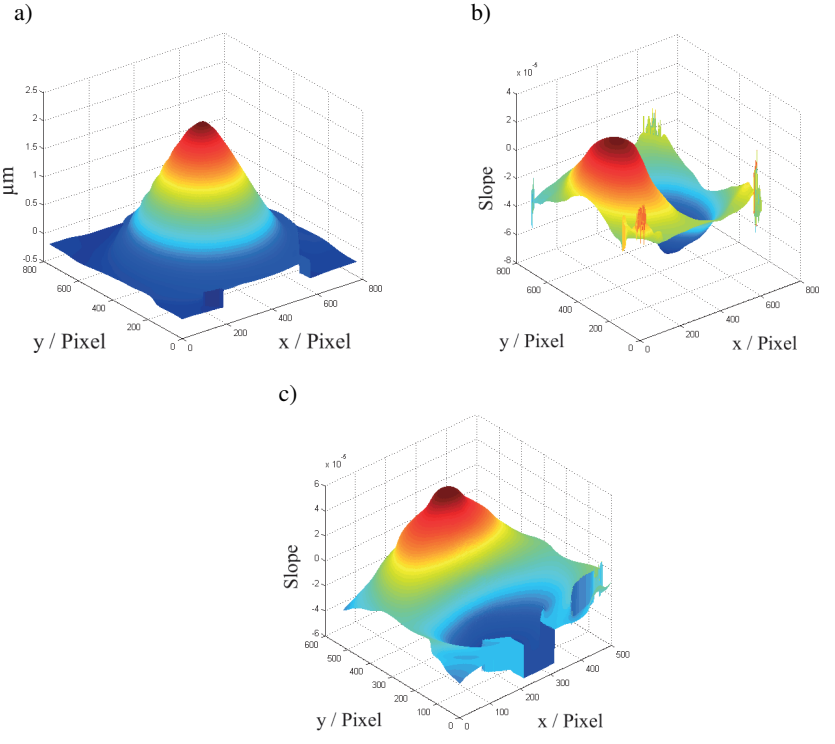

Fig. 5. Continuous three-dimensional distributions: a) w-field; b) $\partial w/\partial x$-field; c) $\partial w/\partial y$-field.

In order to validate the measurement accuracy of the proposed setup, the theoretical result of the circular plate is taken into consideration for comparison. Here, only the out-of-plane displacement is compared. According to the elastic mechanics, the deflection distribution of a circular thin plate, which is subjected to a centrally concentrated loading and clamped along its edges, can be expressed as [25]:

$$w(x,y) = w_{\max}\left(1 - \frac{x^2+y^2}{r^2} + \frac{x^2+y^2}{r^2}\ln\frac{x^2+y^2}{r^2}\right) \qquad \left(\sqrt{x^2+y^2} \le r\right), \tag{7}$$

where $w_{\max}$ is a central deflection of the plate, r is a radius of the plate.

By substituting the experimental parameters, $w_{\max} = 2.2\ \mu$m, $r = 50$ mm, into Eq. (7), the theoretical out-of-plane displacement distribution of the thin plate is hereby obtained. For comparison purpose, the out-of-plane displacement data in the horizontal central cross-section of Fig. 5a are selected. The comparison result between the theoretical and experimental data is shown in Fig. 6. It indicates that the maximum relative error appears at the centre of the plate, and is about 2.3%. It can be seen that the experimental results agree well with those obtained from the theoretical analysis.

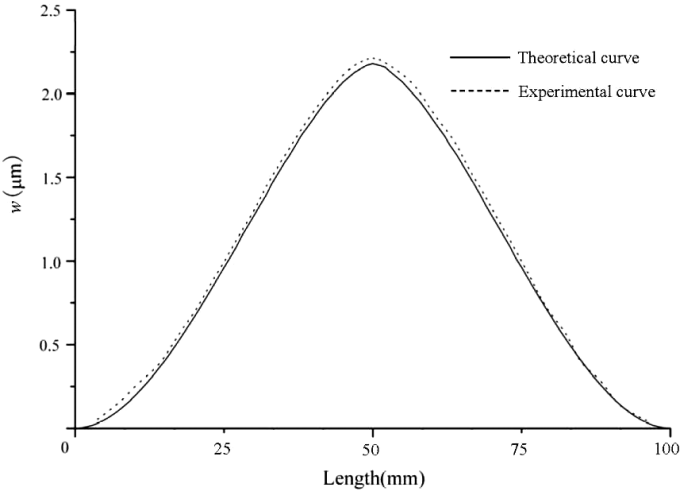

Fig. 6. Comparison of the experimental and theoretical results.

4. NDT application

This section shows the application of a non-destructive testing (NDT) under continuous thermal loading. The tested specimen was a circular aluminium alloy thin plate with a thickness of 6 mm and a radius of 50 mm, as shown in Fig. 7. Two circular-shaped internal defects with the same radius and different embedding depths were prefabricated within the specimen. One defect was located at the left of the plate and was distant by 4 mm from the specimen surface, while the other defect was located at the right of the plate and was distant by 2 mm from the specimen surface. The plate was then thermally loaded with a heat gun. A series of speckle fringe patterns, which can reveal the defects dynamically, were then synchronously captured by three CCD cameras during the procedure of temperature changes.

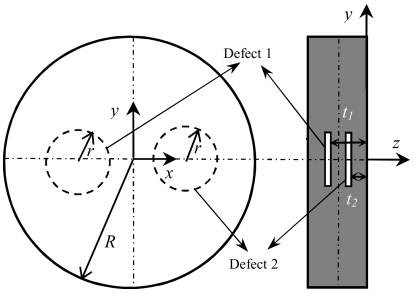

Fig. 7. A schematic of the specimen with defects (left: frontal view; right: side view).

Fig. 8 shows the dynamic non-destructive detection results of the thermally loaded plate, in which two defects' locations are indicated by red arrows. The speckle fringe patterns due to the out-of-plane displacement and its orthogonal slopes are recorded in real time, when the

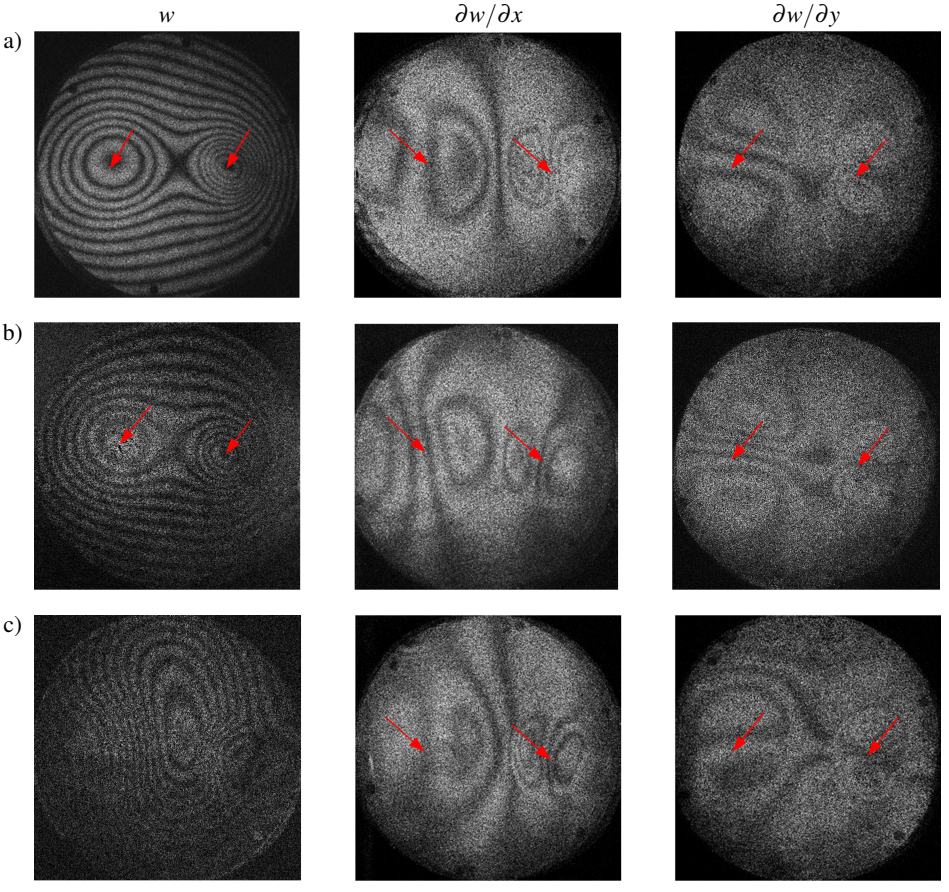

Fig. 8. Dynamic detection results in a continuous heat loading process: the speckle fringe patterns due to the out-of-plane displacement shown in the first column and its orthogonal slopes shown in the second and third columns are recorded at a) $t = 5$ s, b) $t = 10$ s, and c) $t = 15$ s.

deformation of the specimen is increased in the loading process. The speckle fringe patterns from top to bottom represent the out-of-plane displacement and its orthogonal slopes corresponding to time slices at 5 s, 10 s, and 15 s, respectively. From the longitudinal comparison of images in Fig. 8, both the out-of-plane displacement and two orthogonal slopes at the defect location grow very fast with increased thermal loading. It can be found that the defect identification capability of DSPI decreases dramatically during the loading process, while one of DSs is still steady. It can be seen from the horizontal comparison of images in Fig. 8 that the fringe density corresponding to the left shallow defect is much lower than the one corresponding to the right deep defect. It can be obviously seen that the deeper a defect is located, the harder it can be clearly detected. It is demonstrated that the experiment results are in good agreement with the actual positions of defects.

The NDT application illustrated above proves the capability of the proposed synchronous triple-optical-path DSPI system of qualitative identification of both shallow and deep defects in continuously changing loading conditions. Besides, with this system, the defects located in orthogonal directions can be detected simultaneously. However, it is not sufficient to find only locations of internal defects. Many other parameters of internal defects, such as their size, shape and depth, need to be determined together. Therefore, the quantitative detection of internal defects using this system will be the task of further research.

5. Conclusions

As both out-of-plane displacement and its orthogonal slopes can be used to evaluate material's mechanical parameters such as curvatures and twists, a novel synchronous triple-optical-path DSPI system is designed in this study to perform the measurement of the out-of-plane displacement and its orthogonal slopes simultaneously and independently. The new system contains three independent interferometers using only one coherent illumination source. The effectiveness and feasibility of the system are successfully proved by the experimental measurement results of a bent thin plate. With this new synchronous triple-optical-path DSPI system, both shallow and deep internal defects can be easily identified with a one-shot measurement. In a word, this system has the following advantages:

1. Simple structure: an out-of-plane interferometer and shearographic interferometers share the same illumination beam, so that the use of complicated beam splitter devices can be avoided in the system.
2. Simultaneous and accurate measurement capability for both out-of-plane displacement and its orthogonal slopes.
3. Simultaneous measurement of two perpendicular directional slopes provides multiple choices for detection of internal defects located in two perpendicular directions.

Acknowledgements

This work was supported by the National Natural Science Foundation of China (Grant No. 51408524), and the Natural Science Foundation of Jiangsu Province, China (Grant No. BK20160437).

References

[1] Periasamy, C., Tippur, H.V. (2013). A full-field reflection-mode digital gradient sensing method for measuring orthogonal slopes and curvatures of thin structures. *Meas. Sci. Technol.*, 24, 025202.

[2] Kulkarni, R., Gorthi, S.S., Rastogi, P. (2014). Measurement of in-plane and out-of-plane displacements and strains using digital holographic moiré. *J. Mod. Opt.*, 61, 755–762.

[3] Sánchez, A.T., Ibarra, M.H.D.T., Santoyo, F.M., Moreno, I. (2010). Digital holographic interferometer using simultaneously three lasers and a single monochrome sensor for 3D displacement measurements. *Opt. Express*, 18, 19867–19875.

[4] Khoo, S.W., Karuppanan, S., Tan, C.S. (2016). A review of surface deformation and strain measurement using two-dimensional digital image correlation. *Metrol. Meas. Syst.*, 23(3), 461–480.

[5] Yu, L.P., Pan, B. (2017). Full-frame, high-speed 3D shape and deformation measurements using stereo-digital image correlation and a single color high-speed camera. *Opt. Lasers Eng.*, 95, 17–25.

[6] Mathia, T.G., Pawlus, P., Wieczorowski, M. (2011). Recent trends in surface metrology. *Wear*, 271, 494–508.

[7] Krolczyk, J.B., Gapinski, B., Krolczyk, G.M., Samardzic, I., Maruda, B.W., Soucek, K., Legutko, S., Nieslony, P., Javadi, Y., Stas, L. (2016). Topographic inspection as a method of weld joint diagnostic. *Tehnicki vjesnik*, 23(1), 301–306.

[8] Lin, C. S., Yang, S. W., Lin, H. L., Li, J. W. (2017). Measurement of surface profile and surface roughness of fibre-optic interconnect by fast Fourier transform. *Metrol. Meas. Syst.*, 24(2), 381–390.

[9] Rastogi, P.K. (2001). *Digital speckle pattern interferometry and related techniques*. John Wiley & Sons, Ltd, England, 141–224.

[10] Yang, L.X., Xie, X., Zhu, L.Q., Wu, S.J., Wang, Y.H. (2014). Review of electronic speckle pattern interferometry (ESPI) for three dimensional displacement measurement. *Chin. J. Mech. Eng.*, 27, 1–13.

[11] Qin, J., Gao, Z., Wang, X., Yang, S.W. (2016). Three-dimensional continuous displacement measurement with temporal speckle pattern interferometry. *Sensors*, 16, 2020.

[12] Jacquot, P. (2008). Speckle interferometry: A review of the principle methods in use for experimental mechanics applications. *Strain*, 44, 57–69.

[13] Ng, T.W. (1995). Digital speckle pattern interferometer for combined measurements of out-of-plane displacement and slope. *Opt. Commun.*, 116, 31–35.

[14] Fomitchov, P. A., Krishnaswamy, S. (1997). A compact dual-purpose camera for shearography and electronic speckle pattern interferometry. *Meas. Sci. Technol.*, 8, 581–583.

[15] Bhaduri, B., Mohan, N.K., Kothiyal, M.P. (2006). A dual-function ESPI system for the measurement of out-of-plane displacement and slope. *Opt. Lasers Eng.*, 44, 637–644.

[16] Mohan, N.K., Saldner, H., Molin, N.E. (1993). Electronic speckle pattern interferometry for simultaneous measurement of out-of-plane displacement and slope. *Opt. Lett.*, 18, 1861–1863.

[17] Bhaduri, B., Mohan, N.K., Kothiyal, M.P. (2007). Simultaneous measurement of out-of-plane displacement and slope using a multiaperture DSPI system and fast Fourier transform. *Appl. Opt.*, 46, 5680–5686.

[18] Xie, X., Xu, N., Sun, J.F., Wang, Y.H., Yang, L.X. (2013). Simultaneous measurement of deformation and the first deriviation with spatial phase-shift digital shearography. *Opt. Commun.*, 286, 277–281.

[19] Lu, M., Wang, S.J., Aulbach, L., Koch, A.W. (2016). Simultaneous displacement and slope measurement in electronic speckle pattern interferometry using ajustable aperture multiplexing. *Appl. Opt.*, 55, 5868–5875.

[20] Bai, P.X., Zhu, F.P., He, X.Y. (2015). Out-of-plane displacement field measurement by shearography. *Opt. Lasers Technol.*, 73, 29–38.

[21] Richoz, G.L., Schajer, G.S. (2016). Simultaneous two-axis shearographic interferomter using multiple wavelengths and a color camera. *Opt. Lasers Eng.*, 77, 143–153.

[22] Wang, Y.H., Gao, X.Y., Xie, X., Wu, S.J., Liu, Y.X., Yang, L.X. (2016). Simultaneous dual directional strain measurement using spatial phase-shift digital shearography. *Opt. Lasers Eng.*, 87, 197–203.

[23] Gu, G.Q., Wang, K.F., Xu, X. (2014). Denoising in digital speckle pattern interferometry using fast discrete curvelet transform. *Imaging Sci. J.*, 62, 106–110.

[24] Ghiglia, D.C., Pritt, M.D. (1998). *Two-dimensional phase unwrapping: theory, algorithms, and software*. NY: John Wiley & Sons, Ltd, 124–162.

[25] Reismann, H. (1988). *Elastic Plates: Theory and Application*. NY: Wiley Inter-science, 121–133.